






JGR Space Physics



RESEARCH ARTICLE

10.1029/2021JA030166

Cutoff Latitudes of Solar Proton Events Measured by GPS Satellites

C. M. van Hazendonk^{1,2,3} , E. Heino^{1,4} , P. T. A. Jiggins⁵ , M. G. G. T. Taylor⁵ ,
N. Partamies^{1,3} , and H. C. J. Mulders²

¹Department of Arctic Geophysics, University Centre in Svalbard, Longyearbyen, Norway, ²Department of Applied Physics, Eindhoven University of Technology, Eindhoven, The Netherlands, ³Birkeland Centre for Space Science, University of Bergen, Bergen, Norway, ⁴Tromsø Geophysical Observatory, The Arctic University of Norway, Tromsø, Norway, ⁵European Space Research and Technology Centre, European Space Agency, Noordwijk, The Netherlands

Key Points:

- A novel normalization method for Global Positioning System (GPS) energetic particle data is provided involving Geostationary Operational Environmental Satellites (GOES) energetic particle data
- A proton cutoff latitude database (2001–2015; 58 solar proton events) based on GPS energetic particle data is created containing 5714 cutoff latitudes
- Cutoff latitude parameterizations as a function of P_{dyn} and geomagnetic indices Kp and Dst are created for six energies between 18 and 115 MeV

Correspondence to:

C. M. van Hazendonk,
charlottva@unis.no

Citation:

van Hazendonk, C. M., Heino, E., Jiggins, P. T. A., Taylor, M. G. G. T., Partamies, N., & Mulders, H. J. C. (2022). Cutoff latitudes of solar proton events measured by GPS satellites. *Journal of Geophysical Research: Space Physics*, 127, e2021JA030166. <https://doi.org/10.1029/2021JA030166>

Received 1 DEC 2021
Accepted 7 MAR 2022

Abstract Solar energetic particles (SEPs), one of the main causes of particle radiation in interplanetary space, can disrupt radio communication, induce spacecraft failures and change the heating and cooling rates in the atmosphere among others. To investigate the impact of SEPs and more specifically solar proton events (SPEs), we established a cutoff latitude database based on energetic particle data from Combined X-ray Dosimeters (CXDs) on board the Global Positioning System (GPS) spacecraft. Introducing a novel normalization method involving proton fluxes from the Geostationary Operational Environmental Satellites enabled us to include the CXD data from its introduction (2001) onwards. The database contains 5714 cutoff latitudes divided over six energies between 18 and 115 MeV which occur during 58 SPEs from 2001 to 2015. Based on the database, a cutoff latitude parameterization as a function of solar wind dynamic pressure and geomagnetic indices Kp and Dst is created for each energy. Moreover, comparisons to previous studies on energetic particle data from the Polar Orbiting Environmental Satellites have been performed to put the GPS data into perspective. A 1–2° poleward offset is found for the GPS based cutoff latitude models, for which several causes are discussed. Furthermore, the limitation of GPS data to geomagnetic latitudes above 60° should be considered. All in all, the usage of the long time span of GPS data in this study combined with its recent release (2016) opens up a new range of studies involving GPS energetic particle data such as investigating long-term trends with respect to our solar cycle or magnetospheric trends.

1. Introduction

Solar energetic particles (SEPs) are a space weather phenomenon resulting from solar eruptions. Large enhancements in SEP fluxes and more specifically proton fluxes are known as solar proton events (SPEs). During SPEs highly energetic particles of solar origin, predominantly protons and electrons, are accelerated at or near the Sun's surface (Reames, 1999). In addition, energetic storm particles, which are accelerated closer to the Earth at the coronal mass ejection shock passage, can contribute to SPEs. The access of particles to the Earth's atmosphere is controlled by the magnetosphere. Due to its dipole nature, assumed by Störmer (1955), particles can enter easiest at the poles. The lowest latitude to which a particle of a certain rigidity (momentum per unit charge) can penetrate is referred to as the cutoff latitude (Kress et al., 2010). Parameters that influence the cutoff latitude are the energy of a particle, geomagnetic conditions, solar wind and the orientation and incidence angle of the detectors among others (Heino, 2019; O'Brien et al., 2018).

Increased radiation levels and ionospheric currents, partly caused by SPEs, pose a threat to both humans in space and airplanes by disrupting high frequency and very high frequency communication due to ionospheric absorption (Neal et al., 2013) and increased radiation doses for humans on board (Durante & Cucinotta, 2011). During radiation storms satellites may experience an increase in single event effects (SEEs), the most severe of which can endanger equipment or even missions through electronic failures whilst less severe effects, which can be corrected, include bit flips (e.g., Jiggins et al., 2019). In addition, the composition of the middle atmosphere changes due to an enhancement in highly reactive species. These species, odd nitrogen (NO_x , defined as the sum of N, NO, and NO_2 (Verronen et al., 2021)) and odd hydrogen (HO_x , defined as the sum of H, OH, and HO_2 molecules (Verronen et al., 2021)), reduce the ozone concentration (Nesse Tyssøy & Stadsnes, 2015). As ozone is the main absorber of ultraviolet radiation in the middle atmosphere, a change in concentration alters the radiative balance and the heating and cooling rates (Heino, 2019). Therefore, the extent of particle propagation

© 2022 The Authors.

This is an open access article under the terms of the [Creative Commons Attribution-NonCommercial License](https://creativecommons.org/licenses/by-nc/4.0/), which permits use, distribution and reproduction in any medium, provided the original work is properly cited and is not used for commercial purposes.

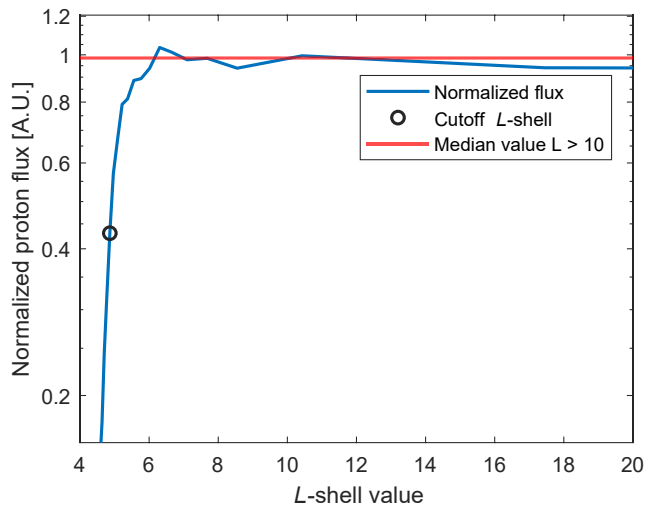


Figure 1. An example of cutoff L -shell determination from Global Positioning System proton fluxes normalized with westward Geostationary Operational Environmental Satellites proton fluxes for $E = 54.99$ MeV.

in the magnetosphere affects a range of space weather impacts and therefore changes in cutoff latitudes should be understood and accurately modeled.

To gain insight in the behavior of cutoff latitudes during various conditions, two main approaches have been used in literature: (a) Numerical calculations by tracing particle trajectories using model magnetospheres; (b) experimental determination based on proton fluxes measured by satellites. The first method has been applied extensively by Smart and Shea (e.g., Smart et al., 1969, 2000; Smart & Shea, 2001, 2003, 2005). A recent example of the back-tracing method in which different magnetic field models are compared is the paper by Boschini et al. (2021). Leske et al. (2001) applied the second method based on data from the Solar Anomalous and Magnetospheric Particle Explorer satellite. The cutoff latitude is determined as the location where the count rate of the proton flux decreased to half of its mean value in the open-field line region. More recent examples of experimental cutoff latitude determination mostly use data from the Polar Orbiting Environmental Satellites (POES) mission (e.g., Birch et al., 2005; Dmitriev et al., 2010; Neal et al., 2013; Nesse Tyssøy et al., 2013; Nesse Tyssøy & Stadsnes, 2015).

In this paper we explore energetic particle data from the Global Positioning System (GPS) satellites (Morley et al., 2017) in combination with data from the Geostationary Operational Environmental Satellites (GOES) network (Onsager et al., 1996) to empirically determine cutoff L -shells during SPEs in the northern hemisphere. In 2017, energetic particle data recorded by Combined X-ray Dosimeters (CXDs) onboard the GPS spacecraft were made publicly available by Los Alamos National Laboratory (LANL) (Morley et al., 2017). The first GPS spacecraft with a CXD instrument was launched in 2001 and nowadays 24 GPS satellites carry a CXD detector. To enable scientific use of the CXD detectors, Carver et al. (2018) cross-calibrated the CXD proton channels with those from the Energetic Particle Sensor (EPS) onboard GOES and found that integral proton fluxes for energies >30 MeV are on average within 20% of each other. In addition, Chen et al. (2020) and Carver et al. (2020) have shown that CXD data can be used to reliably determine cutoff L -shells of solar energetic protons during SPEs by normalizing the proton flux with the average flux in the open field line ($L > 10$) region measured by CXD instruments at each moment. However, in order to apply this method, there should be at least one GPS satellite equipped with a CXD instrument in the open field line region during all times. This requirement is only fulfilled from roughly solar cycle 24 (2009) onwards and earlier energetic particle data from the GPS constellation can thus not be used for cutoff L -shell determination due to a lack of normalization. Supplementing the CXD (GPS) data with EPS (GOES) data enables an extension backwards in time to 2001, more than doubling the time period of the data set and capturing much more SPEs. Therefore, we propose and validate a different normalization method involving data from the EPS onboard of GOES spacecraft to perform a long duration (2001–2015) statistical study of the cutoff L -shells from the GPS constellation. Empirical models for different energies are made using backwards regression. Finally, these empirical models are placed into perspective by providing a comparison with POES based models from Neal et al. (2013) and Nesse Tyssøy and Stadsnes (2015).

2. Instrumentation and Data

2.1. GPS Satellite Data

The GPS spacecraft are divided over six orbital planes with a nominal inclination of 55° above the equator. They have nearly circular orbits at $\sim 20,200$ km altitude with a period of ~ 12 hr. In this period, the satellite moves through the full range of L -shell values four times (twice from low (equatorward) to high (poleward) and vice versa), resulting in one cutoff latitude measurement of $\sim 2.5 - 3$ hr. The lowest reachable L -shell is $L \sim 4$. Between 2001 and 2015, the number of CXD instruments on board GPS spacecraft increased from 1 to 19 and for this period a total of ~ 118 spacecraft years of CXD data is available at <https://www.ngdc.noaa.gov/stp/space-weather/satellite-data/satellite-systems/gps/> (version v1.08 is used for this paper). More information on the actual spacecraft can be found in Morley et al. (2016; Figure 1 and Table 1). The GPS proton data has a time resolution of 4 min. Due to the inclined orbit of the GPS satellites, the latitude range covered in 4 min fluctuates depending on the location of the satellite. In more than 50% of the cases the difference in magnetic latitude between

Table 1
Breakdown of Determined Cutoff *L*-Shells Per Energy

Energy [MeV]	Number of cutoff <i>L</i> -shells
18.18	970
26.30	1400
38.03	1422
54.99	1023
79.53	595
115	304

two measurements is less than 0.1° . For the orbital information, the *L*-shell parameter based on the International Geomagnetic Reference Field (IGRF) and the Tsyganenko 1989 (T89) external field is used.

The CXD instrument onboard the GPS spacecraft consists of three sub-systems containing 6 proton channels (>6 MeV). The omnidirectional detectors have angles of incidence, θ , of $\pm 110^\circ$ ($E = 6 - 50$ MeV) and $\pm 55^\circ$ ($E > 16$ MeV). More information on the different sub-systems can be found in Cayton (2004), Distel et al. (1999) and Tuszewski et al. (2004).

2.2. Other Data Sources

To account for changing geomagnetic conditions in one cutoff latitude measurement, GPS proton fluxes were normalized. Westward-looking (gyrocenter protons at $L > 7$ (Rodriguez et al., 2010)) EPS instruments onboard of GOES spacecraft were used. The GOES location is in geostationary orbit at approximately 35,800 km from the Earth's surface on the equatorial plane. The energy of the seven proton channels of the EPS range from 1.76 to 148 MeV. The spectra are resolved every 5 min. More information on EPS can be found in Onsager et al. (1996). The European Space Agency's (ESA's) Solar Energetic Particle Environment Modeling (SEP-EM) interpolated the proton channels into 11 energy bins for which background fluxes are subtracted and spikes and other corrupted data have been removed or corrected. The data set is available at http://sepem.eu/help/SEP-EM_RDS_v2-01.zip. In this study, the interpolated energy values of 18.18, 26.30, 38.03, 54.99, 79.53 and 115 MeV were used to determine cutoff latitudes.

To model correlation between geomagnetic conditions and cutoff *L*-shell behavior, the geomagnetic indices *K_p* and *D_{st}* as well as the dynamic pressure of the solar wind, P_{dyn} , were used. Experimental studies have shown correlation with *K_p* (Neal et al., 2013), *D_{st}* (Birch et al., 2005; Leske et al., 2001; Nesse Tyssøy et al., 2013) and P_{dyn} (Nesse Tyssøy & Stadsnes, 2015). For our study, geomagnetic indices have been retrieved from the World Data Center (WDC) for Geomagnetism, Kyoto (<http://wdc.kugi.kyoto-u.ac.jp/wdc/Sec3.html>) (Matzka et al., 2021; Nose et al., 2015) and P_{dyn} from Omniweb (https://omniweb.gsfc.nasa.gov/form/omni_min.html).

2.3. Solar Proton Events

A SPE is defined by the National Oceanic and Atmospheric Administration (NOAA) when the GOES proton flux >10 MeV integral value exceeds 10 particles $\text{cm}^{-2}\text{s}^{-1}\text{sr}^{-1}$ (10 pfu). The integral flux data of GOES is available at <https://www.ngdc.noaa.gov/stp/satellite/goes/>. The start and end times of the SPEs between 2001 and 2015 for which cutoff *L*-shells were found are listed in Table A1 together with the peak flux of each SPE, the number of CXD instruments available and the number of cutoff *L*-shells determined. To avoid short SPEs and/or SPEs with no significant high-energy flux components penetrating the Earth's atmosphere, only SPEs with at least one cutoff *L*-shell per available CXD detector for the 38.03 MeV energy are taken into account.

3. Methods

For normalization, the 4-min GPS proton data is matched with the closest point in time of the 5-min GOES proton data. Similar to previous studies (Carver et al., 2020; Chen et al., 2020; Leske et al., 2001), the cutoff *L*-shell is determined for each individual satellite at the location at which the normalized proton flux is closest to half (and within 45%–55%) of its median value in the open-field line region ($L > 10$). To ensure data quality of the cutoff *L*-shells, several constraints are added: (a) Minimum of 6 data points in open-field line region for a reliable median; (b) the median in the open-field line region, which is expected to equal 1, should at least have a value between 0.5 and 1.5 to remove periods where the cross-correlation between GPS and GOES fluxes is insufficient; (c) removal of cutoff *L*-shells with $L > 7.5$ due to high variability (Neal et al., 2013); (d) removal of maximum proton fluxes exceeding two times the median value in $L > 10$; (e) removal of proton fluxes with a standard deviation in the open-field line region exceeding $2 \times \frac{18.18}{E}$, where E [MeV] represents the energy of the proton channel and 18.18 MeV refers to the lowest energy channel considered. Constraints (4) and (e) both avoid highly fluctuating proton fluxes, which can for example, occur at SPE onsets with rapid changes in proton flux.

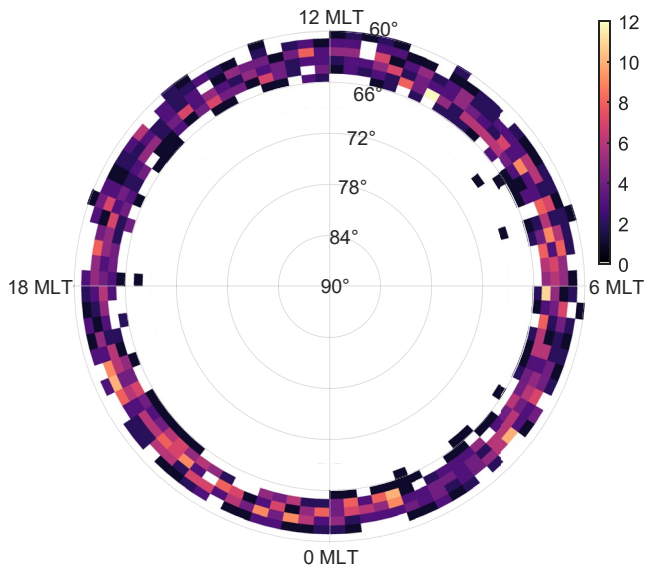


Figure 2. Distribution of cutoff latitudes over magnetic local time (MLT) sectors for $E = 38.03$ MeV. Magnetic latitude is depicted on the radial axis and MLT in the theta direction with bin sizes 1° and 15 min respectively. The distribution looks comparable for other energies.

In Figure 1, an example of cutoff L -shell determination is shown. Applying the algorithm to all SPEs between 2001 and 2015 results in a database of 5714 cutoff L -shells. The breakdown over the six energies and the distribution over the SPEs are shown in Table 1 and A1 respectively. For $E = 38.03$ MeV the distribution of cutoff latitudes, λ_c (magnetic latitude (MLAT)), over all magnetic local time (MLT) sectors is shown in Figure 2 with bin sizes $\Delta\theta = 3.75^\circ$ (15 min) and $\Delta r = 1^\circ$ MLAT. For conversion from cutoff L -shell to cutoff latitude the relation $\lambda_c = \cos^{-1} \left(\sqrt{\frac{1}{L_{\text{shell}}}} \right)$ is used.

4. Results and Discussion

4.1. Validation Normalization Method

To validate the novel normalization method, both a visual comparison of the January 2014 event (peak >10 MeV flux of 1033 pfu) as published by Carver et al. (2020) in Figure 11 and a quantitative comparison of the entire cutoff L -shell database are performed.

Figure 11 from Carver et al. (2020) has been used as the benchmark for visual comparison and we duplicate that approach in Figure 3. Figure 3 (a) shows the non-normalized >10 MeV integral fluxes with bin sizes $\Delta L = 0.2$ and 90 min during the January 2014 SPE. Light gray bins represent bins without data. As no normalization is applied, similar results to Figures 11 (top) of Carver et al. (2020) are expected and observed. In Figure 3 (b) the $E = 38.03$ MeV differential flux has been normalized using GOES proton data. White bins represent a normalized proton flux between 0.4 and 0.6 indicating the cutoff location as applied by Carver et al. (2020). Note that a more precise definition between 0.45 and 0.55 is used for the database in this paper as described in Section 3. On top, cutoff L -shell values from the database created in this paper are plotted in black. Similar behavior can be observed when comparing panel (b) to Figures 11 (bottom) by Carver et al. (2020), however direct comparison of the specific cutoff location is not valid due to different energies.

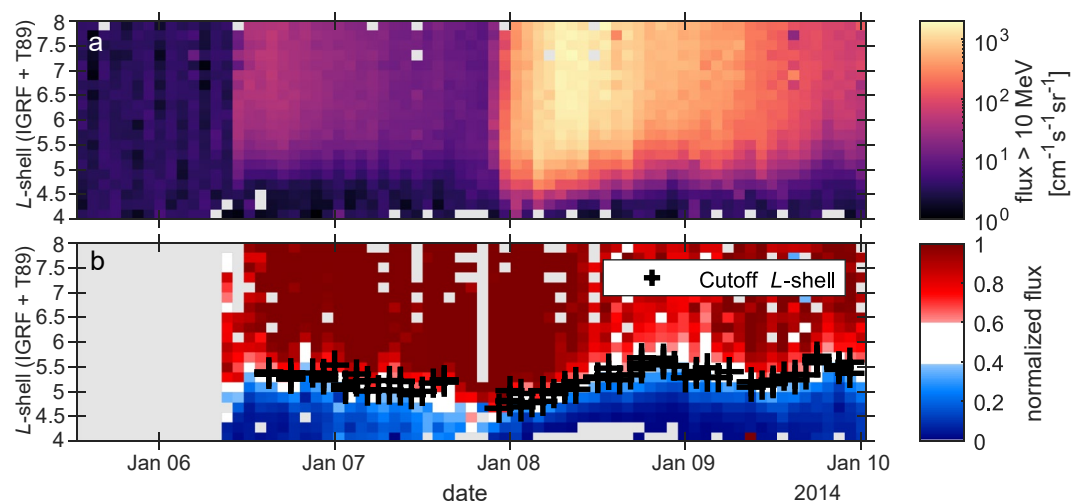


Figure 3. Proton fluxes during the January 2014 solar proton event with bin sizes $\Delta L = 0.2$ and 90 min. Light gray bins represent bins without data. Panel (a) non-normalized >10 MeV integral proton fluxes. Panel (b) $E = 38.03$ MeV, normalization method involving Geostationary Operational Environmental Satellites proton fluxes. The white bins indicate the location of the cutoff L -shells defined between 40%–60% of the proton flux in the open-field line region as applied by Carver et al. (2020). Black plus-signs indicate locations of cutoff L -shells as determined in this paper. This figure uses the same layout and visual comparison approach as Figure 11, published by Carver et al. (2020).

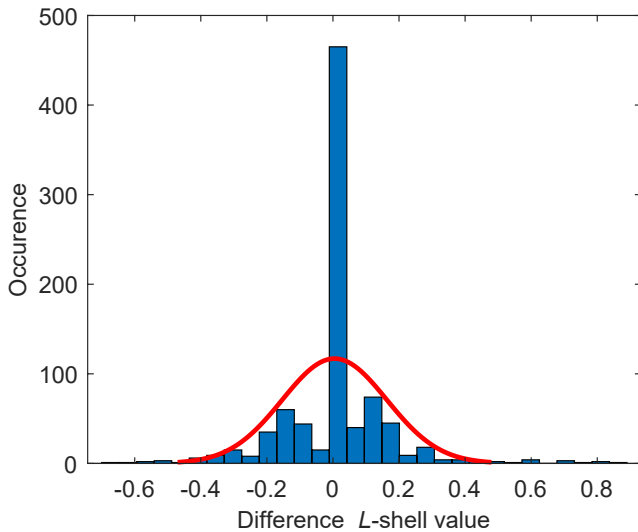


Figure 4. Difference in L -shell value based on 876 linked cutoff L -shells for $E = 38.03$ MeV with a Gaussian distribution fitted on top in red ($\mu = 0.0048$ and $\sigma = 0.16$). The difference percentage between the two normalization methods is 1.8%.

For a quantitative comparison, both normalization methods have been used to calculate cutoff L -shells and values from both methods have been linked for the same satellite within a 60-min time interval. The difference in L -shell for all cutoffs has been plotted for $E = 38.03$ MeV in Figure 4 with a Gaussian distribution on top in red with a mean, μ , of 0.0048 and a standard deviation, σ , of 0.16. The mean difference in L value between both normalization methods is listed in Table 2 for each energy with the difference percentage and the number of linked cutoffs per energy. In agreement with the cross-correlation determined by Carver et al. (2018), the difference percentage is smallest (<2%) when $E > 30$ MeV. For higher energies, fewer cutoff L -shells are linked due to GOES differential fluxes becoming zero for both less intense SPEs and less intense periods of SPEs. The low difference percentage in combination with the switching minus and plus sign of mean difference leads to the conclusion that the normalization method involving GOES energetic particle data can be implemented.

4.2. Cutoff Latitude Variations With Geomagnetic Activity

To understand cutoff L -shell behavior and variation in relation to geomagnetic activity, we empirically model different geomagnetic parameters. Univariate regression first determines the main driving characteristics resulting in the Dst and Kp indices and the dynamic pressure of the solar wind, P_{dyn} [nPa], as initial parameters for the backward regression procedure. In case of

the Kp index, both Kp_{shift} and Kp_{shift}^2 , which are 3 hr shifted forward in time, are used due to their higher correlation values. The 3 hr shift has been applied by Neal et al. (2013) previously. The location of the magnetopause is determined by the pressure balance between P_{dyn} and the pressure inside the magnetopause, resulting in a relation between the magnetopause location and $P_{dyn}^{-1/6}$ (Ganushkina et al., 2018). On the other hand, Nesse Tyssøy and Stadsnes (2015) report an optimal correlation for the cutoff latitude and $P_{dyn}^{1/3}$. In this study, results are slightly better when P_{dyn} to the power of 1/3 is applied.

For the backward selection multivariate linear regression is performed for all six energies separately. The variable with the highest P -value is left out in the next iteration. In the end, the optimal relation is the parameterization with the highest R_{adj}^2 value for which all P -values are below 0.05. Since the L -shell parameter is not a linear variable, a switch to cutoff latitude, λ_c , has been made for the backward regression. The relation to empirically determine the cutoff latitude (based on the IGRF internal and T89 external magnetic field models) at the start of the backwards selection is given by

$$\text{Cutoff latitude (IGRF + T89)} = ADst + BP_{dyn}^{1/3} + CKp_{shift} + DKp_{shift}^2 + E, \quad (1)$$

in which A , B , C , D and E are regression coefficients. The coefficients of the optimal parameterization for each energy as well as the adjusted coefficient of determination, R_{adj}^2 , and the Root Mean Square Error (RMSE) which gives the standard deviation of the residuals are displayed in Table 3. The models for all six energies are plotted in Figure 5a. As expected, higher energies penetrate further equatorward. In addition, the geomagnetic parameters used for the models are plotted in Figures 5b and 5c.

The discrepancy in the coefficient of determination compared to previous literature (R^2 values between 0.4 and 0.6 (Leske et al., 2001; Neal et al., 2013; Nesse Tyssøy et al., 2013)) partly arises from the incorporation of the T89 external field model in the cutoff latitude calculations. As the external field model adjusts for geomagnetic disturbances, the correlation is less pronounced. When the parameterizations are determined as a function of IGRF dependent cutoff latitude, λ_c , Table 3 becomes Table 4. In addition, the energies below 54.99 MeV show lower correlation. This is presumably caused by the fact that the normalized fluxes are zero during less intense

Table 2
Mean Difference Percentage in L Value Between the Two Normalization Methods

Energy [MeV]	Mean difference	Difference percentage	Data points
18.18	0.0128	2.8	475
26.30	-0.0070	2.2	761
38.03	0.0048	1.8	876
54.99	-0.0042	1.5	624
79.53	0.0051	1.3	376
115	0.0072	1.8	178

Table 3
Empirical Fitting Parameters for Equation 1 for Each Energy, the Adjusted Coefficient of Determination R_{adj}^2 and the Root Mean Square Error for Each Fitting

Energy [MeV]	A	B	C	D	E	R_{adj}^2	RMSE
18.18	0.0075	-1.0393	-0.3021	0.0281	65.6928	0.2305	1.0462
26.30		-0.7273	-0.5354	0.0471	65.3694	0.2619	1.0044
38.03	0.0034	-0.7769	-0.5307	0.0550	65.2463	0.3088	0.9013
54.99		-0.4392	-0.6391	0.0607	64.7626	0.3514	0.8059
79.53	0.0088	-0.7880	-0.4412	0.0574	64.7112	0.3645	0.6878
115	0.0069	-0.6030	-0.3920	0.0537	63.9058	0.2429	0.7224

Note. The number of data points per energy is given in Table 1.

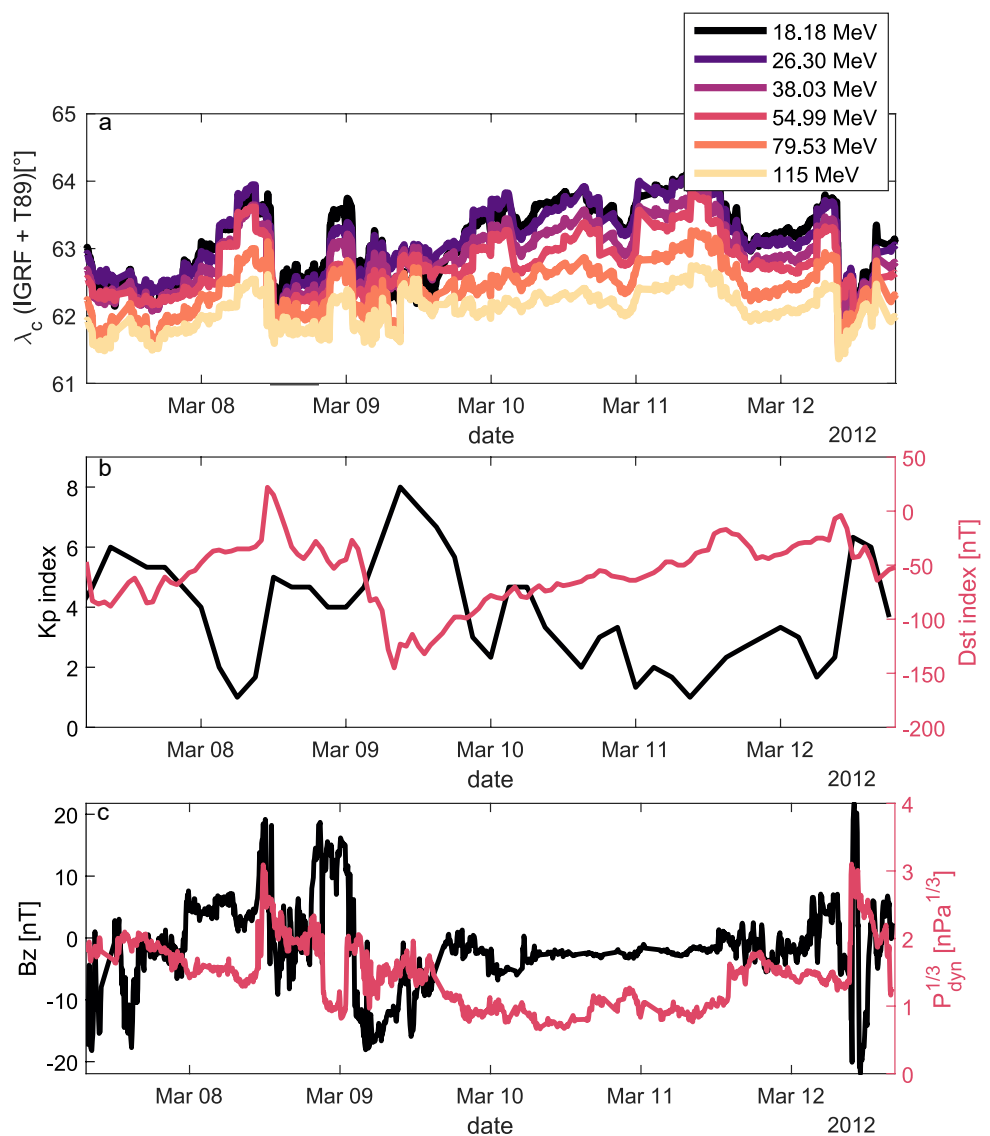


Figure 5. Visualizations for the solar proton event of 7–12 March 2012 with tic marks on the x-axis located at 00 Universal Time (UT) each day. Panel a displays a comparison of empirical models obtained for six different energies. Panel b shows the shifted K_p (black) and Dst (pink) indices. Panel c shows the B_z component of the Interplanetary Magnetic Field (IMF) (black) and $P_{dyn}^{1/3}$ (pink).

Table 4

Empirical Fitting Parameters When the Cutoff Latitude (International Geomagnetic Reference Field (IGRF) + T89) in Equation 1 is Replaced by Cutoff Latitude (IGRF) for Each Energy, the Adjusted Coefficient of Determination R^2_{adj} and the Root Mean Square Error for Each Fitting

Energy [MeV]	A	B	C	D	E	R^2_{adj}	RMSE
18.18	0.0080	-1.1641	-0.3711	0.0305	65.5269	0.3024	1.0509
26.30		-0.7475	-0.5966	0.0457	65.0922	0.3251	1.0177
38.03	0.0042	-0.8651	-0.6089	0.0607	65.0746	0.3729	0.9180
54.99	0.0033	-0.6050	-0.6522	0.0603	64.6616	0.4296	0.8126
79.53	0.0091	-0.8262	-0.4758	0.0511	64.4651	0.4463	0.7008
115	0.0068	-0.6210	-0.3984	0.0418	63.6381	0.3487	0.7174

Note. The number of data points per energy is given in Table 1.

moments of SPEs for the higher energies. Setting the normalized fluxes of 18.18, 26.30 and 38.03 MeV to zero when the 54.99 MeV normalized flux is zero, results in R^2_{adj} values of 0.3909, 0.4106 and 0.4466 respectively.

Another contribution to lower correlation values would arise from large number of SPEs (58) used in this study as well as their various strengths and driving mechanisms. Leske et al. (2001) and Nesse Tyssøy and Stadsnes (2015) only used six SPEs with peak >10 MeV fluxes above 350 pfu and 1000 pfu respectively. Neal et al. (2013) restrict themselves to 15 SPEs with peak >10 MeV fluxes above 350 pfu. In addition, Neal et al. (2013) remove the periods impacted by Interplanetary Coronal Mass Ejection (ICME) arrivals (15 min and 6 hr after arrival of the ICME impulse), which implies that their model might not work optimally during the peak fluxes associated with ICME arrival.

4.3. Comparison Empirical Models With Previous Literature

To place this first empirical model based on data from GPS spacecraft in perspective, a comparison with two other empirical models based on POES spacecraft by Neal et al. (2013) and Nesse Tyssøy and Stadsnes (2015) is performed.

For comparison to Neal et al. (2013), the regression formula

$$\lambda_c \text{ (IGRF)} = AKp_{shift}^2 + BKp_{shift} + C, \quad (2)$$

in which λ_c is the cutoff latitude (MLAT) and A, B and C are regression coefficients is used. In addition, procedures from Neal et al. (2013) (removal of cutoff latitudes above 66°, only 15 SPEs, removal of ICME impacts and use of cutoff latitude (IGRF) [MLAT]) are applied to the GPS database as well. The results of the comparison of the 24.3 and 51.5 MeV (energy value at the satellite) (Neal et al., 2013) to the respectively 26.30 and 54.99 MeV GPS channel are summarized in Table 5 and Figures 6a and 6b. The grey area in these Figures represents the ICME impact period (10:50–17:05 UT 8 March 2012) for which the cutoff latitudes have not been included in the models.

Table 5

Comparison of the Empirical Model of Neal et al. (2013) and the Global Positioning System Based Empirical Model Determined in This Paper

Model	Energy (MeV)	A	B	C	R^2	RMSE	Data points
Neal et al. (2013)	24.3	-0.057912	-0.38237	63.1626	0.50154	1.72 ^a	7683
GPS based data	26.30	0.0294	-0.6003	64.3863	0.4071	0.8752	490
Neal et al. (2013)	51.5	-0.08087	-0.14163	61.712	0.6216	1.3243 ^a	4620
GPS based data	54.99	0.0252	-0.5291	63.7603	0.4537	0.7242	471

^aNeal et al. (2013) define the given error as the estimate of the standard deviation of the error. This is interpreted as the RSME in this paper.

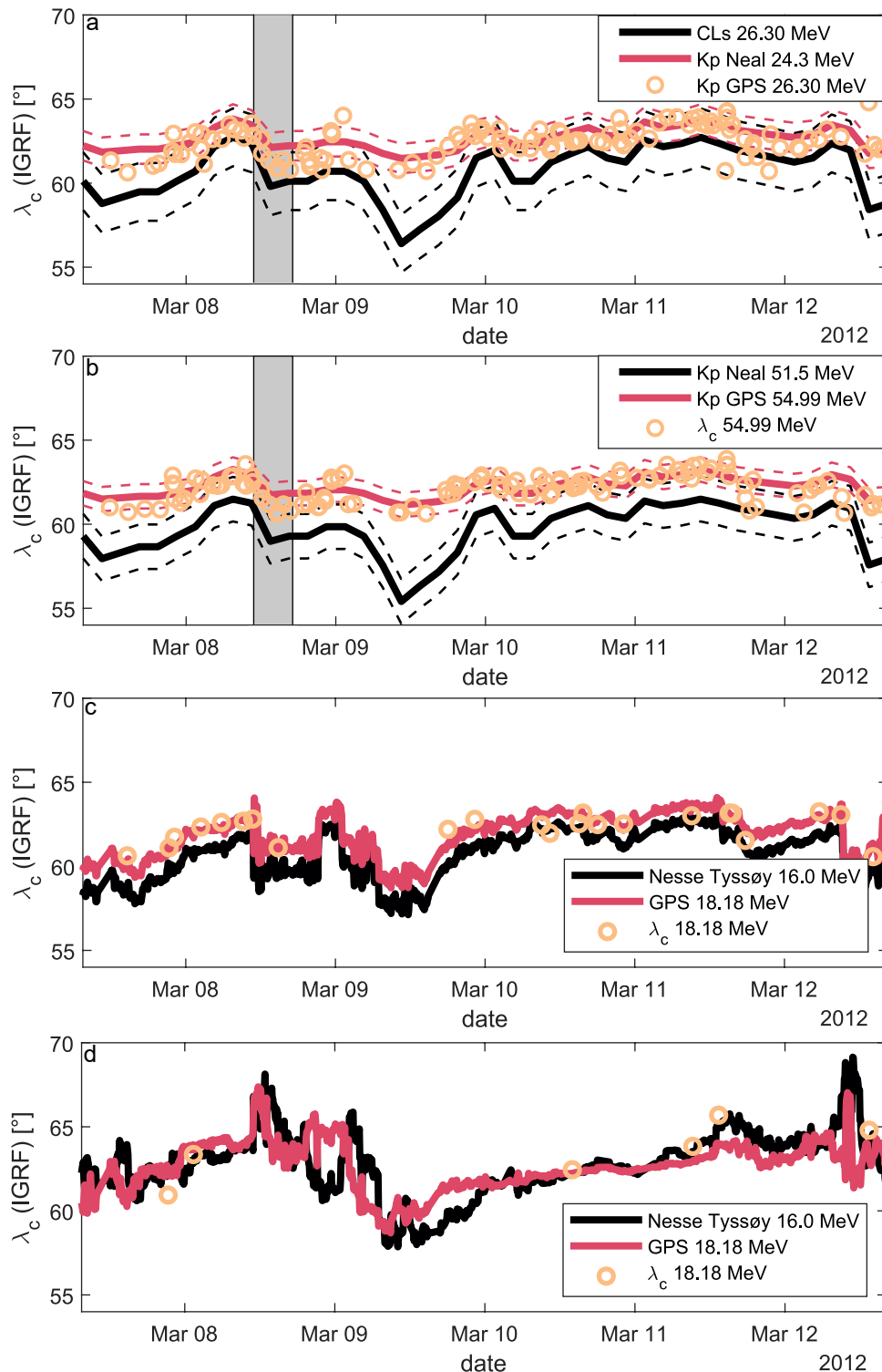


Figure 6. Comparison of empirical models from literature (black) and the Global Positioning System (GPS) cutoff latitude database (pink) with cutoff latitudes from the database plotted in circles. The cutoff latitude is plotted for the March 2012 solar proton event. The tic marks on the x-axis are located at 00 Universal Time (UT) each day. The dashed lines display the Root Mean Square Error. The gray background (10:50–17:05 UT 8 March 2012) represents the period of Interplanetary Coronal Mass Ejection arrival (impulse time at 11:05 UT 8 March 2012) not taken into account by the K_p based model from Neal et al. (2013) and the comparison models from this paper in panels (a and b) Panel (a) 24.3 MeV (Neal et al., 2013) versus 26.30 MeV (GPS database) as given by the parameterization in Equation 2. Panel (b) 51.5 MeV (Neal et al., 2013) versus 54.99 MeV (GPS database) as given by the parameterization in Equation 2. Panel (c) nightside 16.0 MeV (Nesse Tyssøy & Stadsnes, 2015) versus nightside 18.18 MeV (GPS database) as given by the parameterization in Equation 3. Panel (d) dayside 16.0 MeV (Nesse Tyssøy & Stadsnes, 2015) versus dayside 18.18 MeV (GPS database) as given by the parameterization in Equation 4.

Table 6

Comparison of the Nightside Empirical Model (Equation 3) of Nesse Tyssøy and Stadsnes (2015) and the Global Positioning System Based Empirical Model Determined in This Paper

Model	Energy [MeV]	A	B	C	R ²	RMSE	Data points
Nesse Tyssøy and Stadsnes (2015)	16	0.035	−3.0	67.0	0.52	^a	^a
GPS based data	18.18	0.027	−2.1	66.5	0.42	0.80	69

^aInformation not provided.

Comparison to Nesse Tyssøy and Stadsnes (2015) has been conducted for the nightside (21–03 MLT) using

$$\lambda_c(\text{CGM latitude}) = ADst + BP_{dyn}^{1/3} + C \quad (3)$$

and for the dayside (09–15 MLT) using

$$\lambda_c(\text{CGM latitude}) = ADst + BB_{Z,N} + C \quad (4)$$

where $\lambda_c(\text{CGM latitude})$ is the cutoff latitude in Corrected GeoMagnetic latitude and $B_{Z,N}$ is the northward component of the Interplanetary Magnetic Field (IMF). Note that the regression coefficients A , B and C are different for both equations. Usage of the same six SPEs and only IGRF dependent cutoff latitudes ensures proper comparison. Since Nesse Tyssøy and Stadsnes (2015) focus on lower energies (1–32 MeV on the dayside and 1–16 MeV on the nightside), their 16 MeV channel has been compared to the 18.18 MeV GPS channel. The results are shown in Tables 6 and 7 and Figures 6c and 6d. Analogously to Section 4.2, removal of the less energetic moments of the SPEs (setting the normalized flux of 18.18 MeV to zero when the 54.99 MeV normalized flux is zero), results in slightly higher R^2 (0.61 for the nightside and 0.45 for the dayside). Again, the geomagnetic parameters for the March 2012 SPE are plotted in Figures 5b and 5c.

In both comparisons, the low number of data points of the GPS database due to long cutoff latitude measurements is a limiting factor. In addition, the lack of GPS data points below $L = 4$ ($\lambda = 60^\circ$) provides an inaccuracy especially during the more powerful SPEs on which the POES models are based. During the peak of the March 2012 event, the most powerful SPE of solar cycle 24 (peak >10 MeV flux 6530 pfu), Figures 6a and 6b clearly show the inability to properly model below 60° . Therefore, it is suggested to supplement GPS energetic particle data with for example, POES energetic particle data especially for modeling higher proton energies.

Another notable difference between the POES based Neal et al. (2013) and GPS parameterizations in Figures 6a and 6b is the offset during the entire SPE. O'Brien et al. (2018) reports a comparable offset for the September 2017 SPE between the empirical models based on POES data on the one hand and the Relativistic Proton Spectrometer (RPS) on board the Van Allen Probes mission on the other hand. This offset is mainly attributed to a discrepancy in the integral energy channels, the calculation of the differential channels and the dependence on angle of incidence. To visualize the offset in this paper, the parabolic difference between both empirical models has been plotted as a function of Kp index in Figure 7a. The steep increase during geomagnetic storm levels can be explained due to the inability to measure below 60° . However, the $\sim 1\text{--}2^\circ$ offset, depending on the energy, during geomagnetic quiet times is not completely understood. To get more insight in the offset during different SPE conditions, Figure 7 shows histograms of the difference in cutoff latitude during all SPEs taken into account for modeling the comparisons to Neal et al. (2013) (15 SPEs; Figure 7b) and to Nesse Tyssøy and Stadsnes (2015) (6 SPEs; Figure 7c (dayside) and 7days (nightside)). Note that the number of data points is dependent on the time

Table 7

Comparison of the Dayside Empirical Model (Equation 4) of Nesse Tyssøy and Stadsnes (2015) and the Global Positioning System Based Empirical Model Determined in This Paper

Model	Energy [MeV]	A	B	C	R ²	RMSE	Data points
Nesse Tyssøy and Stadsnes (2015)	16	0.070	0.14	66.5	0.53	^a	^a
GPS based data	18.18	0.027	0.10	64.5	0.35	0.97	49

^aInformation not provided.

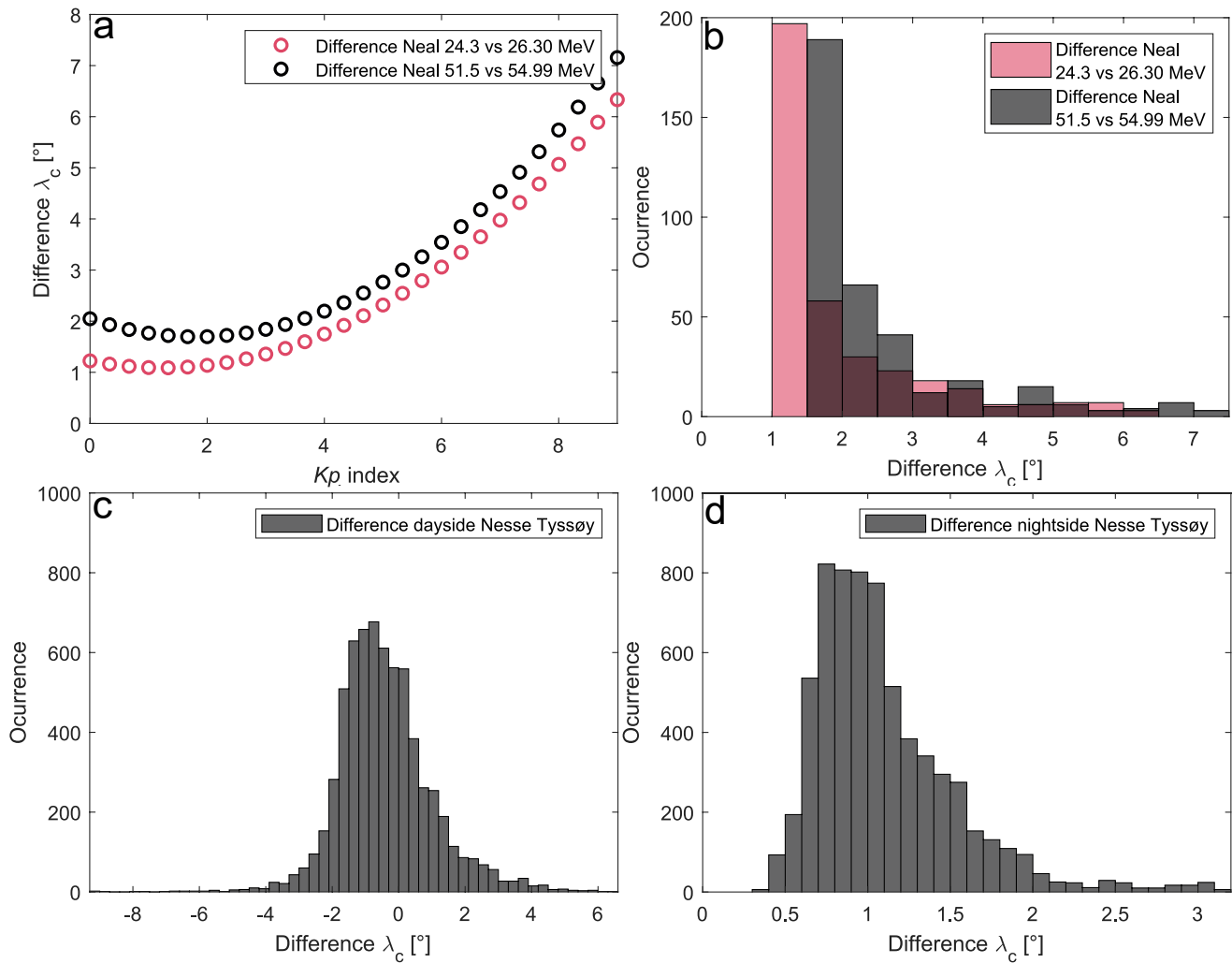


Figure 7. Panel (a) the difference in cutoff latitude plotted as a function of the Kp index when Equation 2 for 24.3 (51.5) MeV (Neal et al., 2013) has been subtracted from the 26.30 (54.99) MeV (Global Positioning System) version. Panel (b) histogram of the difference between the parameterization of 24.3 (51.5) MeV Neal et al. (2013) and the 26.30 (54.99) MeV empirical model from this paper. The same 15 solar proton events (SPEs) as during the modeling have been taken into account with data points each 3 hr. Panel (c) histogram of the difference between the dayside parameterization of 16.0 MeV Nesse Tyssøy and Stadsnes (2015) and the 18.18 MeV empirical model from this paper. The same 6 SPEs as during the modeling have been taken into account with data points every 5 min. Panel (d) Same procedure as panel (c) comparing the nightside parameterizations instead of the dayside ones.

resolution of the parameterizations (3 hr for Figure 7b vs. 5 min for Figures 7c and 7d). The difference seems larger for higher energies (the 51.5 and 54.99 MeV energies in Figures 7a and 7b) than lower energies (Figures 7c and 7d). Please note that the lower energies have an additional uncertainty due to a reduced cross-correlation between the GPS and GOES proton fluxes for $E < 30$ MeV as discussed in Section 1. When comparing the day- and nightside, the deeper penetration on the nightside comes with a larger offset between the GPS and Nesse Tyssøy and Stadsnes (2015) empirical models.

Possible contributions to the offset are: (a) Broader energy channels POES satellites (center value 51.5 MeV corresponds to the 35–70 MeV passband) and a mismatch of the integral energy channels; (b) opposite orientation of the detectors: Zenith (POES) versus nadir (GPS). Contribution (1) could indicate that it would be more accurate to compare the upper limit of a POES passband to the differential GPS energy as well as calibrate the POES and GPS energy channels against each other. Contribution (2) involves the dependence of the cutoff latitude on the angle of incidence. Both POES and GPS spacecraft have omnidirectional detectors with an angle of incidence of $\pm 60^\circ$ (POES > 16 MeV), $\pm 110^\circ$ (GPS 6–50 MeV channel) and $\pm 55^\circ$ (GPS > 16 MeV channels). In addition, POES has two directional (nadir and 90° from nadir) telescopes for lower proton energies. Omnidirectionality suggests that the detectors may blend together cutoff latitudes with different angles of incidence, meaning that

several proton gyrocenter locations, λ_{GC} , are measured at the same spacecraft location, λ_{SC} . Due to the opposite orientation, the blends might be different where zenith orientation (POES) has a tendency that λ_{GC} can be larger than λ_{SC} , whereas nadir orientation (GPS) might have the opposite effect. This would result in POES based models estimating the cutoff latitude too far equatorward, while GPS based models exhibit a poleward shift.

Suggestions for implementation of the GPS based cutoff latitude models include among others: (a) Verification and improvement of POES based models by resolving the cause of the offset in latitude and thus finding a more precise cutoff latitude location; and (b) implementation of the GPS based (or a combination of GPS and POES based) models in climate models. Nowadays, the assumption of a spatially uniform energetic proton precipitation above 60° geomagnetic latitude is made in climate models during SPEs (Matthes et al., 2017). The GPS (and/or POES) based models can provide a more accurate estimation of the real area affected by energy precipitation.

5. Conclusions and Summary

The long time period in combination with the large number of available CXD instruments make the GPS energetic particle data an important tool to monitor and understand solar proton behavior during SPEs. In this paper we have demonstrated the potential of GPS energetic particle data by: (a) Introducing and validating a new normalization method involving GOES energetic particle data; (b) creating a cutoff latitude database from 2001 to 2015 existing of over 5700 cutoff latitudes; (c) empirically modeling the cutoff latitude as a function of Dst , Kp_{shift} , Kp_{shift}^2 and P_{dyn} for six energies ranging from 18 to 115 MeV; and (d) comparing the empirical models to POES based empirical models from Neal et al. (2013) and Nesse Tyssøy and Stadsnes (2015).

When using GPS energetic particle data it is important to take into account that the data coverage is limited to geomagnetic latitudes above 60°. This may underestimate the proton fluxes during the most intense SPEs. Furthermore, more research is needed to draw solid conclusions on the offsets (about 1–2° poleward) between the empirical cutoff latitude model based on GPS and POES. Despite these shortcomings we find the GPS based model helpful in understanding and resolving the proton cutoff latitude behavior. The demonstration of the long term potential of the CXD data in this work opens up possibilities for future use looking for example, at long term trends with respect to the solar cycle or other magnetospheric phenomena.

Appendix A: SPEs List

Table A1

List of Solar Proton Events With Their Start and End Time and Maximum Flux Between March 2001 and December 2015 for Which Cutoff L-Shells Are Found

Start time	End time	Maximum >10 MeV proton flux (pfu)	Number of CXDs	Cutoff L-shells
29-03-01 16:35	31-03-01 06:35	35.4	1	15
02-04-01 23:40	06-04-01 13:00	1110	1	40
10-04-01 08:50	13-04-01 10:00	355	1	40
15-04-01 14:10	17-04-01 15:55	951	1	18
18-04-01 03:15	20-04-01 07:20	321	1	27
15-06-01 17:50	16-06-01 11:25	26.8	1	2
16-08-01 01:35	18-08-01 05:40	493	1	12
24-09-01 12:15	30-09-01 08:20	12900	1	39
01-10-01 10:45	05-10-01 01:55	2360	1	24
04-11-01 17:05	09-11-01 15:05	31700	1	53
22-11-01 23:20	26-11-01 22:15	18900	1	36
26-11-01 22:55	27-11-01 12:10	17	1	3
26-12-01 06:05	28-12-01 05:15	780	1	24
30-12-01 21:20	04-01-02 19:20	108	1	43
10-01-02 20:45	13-01-02 13:05	91.8	1	25
18-03-02 13:20	19-03-02 20:25	53.1	1	12

Table A1
Continued

Start time	End time	Maximum >10 MeV proton flux (pfu)	Number of CXDs	Cutoff <i>L</i> -shells
21-04-02 02:25	25-04-02 18:30	2520	1	27
22-05-02 17:55	24-05-02 13:15	820	1	10
16-07-02 17:50	18-07-02 12:40	234	1	4
22-07-02 06:55	26-07-02 01:15	28.5	1	23
22-08-02 04:40	22-08-02 23:15	36.4	1	7
24-08-02 01:40	26-08-02 12:10	317	1	14
09-11-02 19:20	11-11-02 05:10	404	1	7
26-10-03 18:25	27-10-03 18:30	466	2	8
28-10-03 12:15	01-11-03 04:00	29500	2	39
02-11-03 11:05	04-11-03 19:40	1570	2	33
04-11-03 22:25	07-11-03 03:05	353	2	38
13-09-04 21:05	15-09-04 04:30	273	4	10
07-11-04 19:10	13-11-04 01:50	495	4	84
16-01-05 02:10	22-01-05 16:15	5040	5	198
14-05-05 05:50	15-05-05 06:35	3140	5	13
16-06-05 22:00	17-06-05 17:00	43.8	5	17
14-07-05 14:00	16-07-05 22:00	134	5	37
27-07-05 23:00	01-08-05 09:45	41.1	5	120
22-08-05 20:40	25-08-05 00:15	337	5	68
08-09-05 02:25	12-09-05 21:30	1880	5	220
14-09-05 00:40	16-09-05 00:25	235	5	38
06-12-06 16:15	12-12-06 10:35	1980	7	368
13-12-06 03:10	14-12-06 21:20	698	7	130
08-03-11 01:05	10-03-11 01:00	50.4	10	64
07-06-11 08:20	08-06-11 15:55	72.9	10	147
04-08-11 06:35	06-08-11 04:25	96.4	11	122
24-09-11 18:35	26-09-11 20:50	35.7	11	66
26-11-11 11:25	28-11-11 00:25	80.3	11	61
23-01-12 05:30	27-01-12 08:50	6314	11	360
27-01-12 19:05	31-01-12 05:20	796	11	325
07-03-12 05:10	12-03-12 19:10	6530	11	605
13-03-12 18:10	15-03-12 06:15	469	11	87
17-05-12 02:10	18-05-12 13:40	255	11	163
17-07-12 17:15	21-07-12 00:00	136	11	80
11-04-13 10:55	12-04-13 18:45	114	12	145
15-05-13 14:20	18-05-13 12:25	41.7	12	126
30-09-13 05:05	02-10-13 04:45	182	13	116
06-01-14 09:15	11-01-14 16:25	1026	13	515
25-02-14 14:50	02-03-14 22:25	103	14	418
18-04-14 15:25	20-04-14 11:50	58.5	14	138
11-09-14 02:55	12-09-14 22:35	126	16	194
21-06-15 20:35	24-06-15 04:45	1066	18	56

Note. The number of available combined X-ray dosimeter instruments and the number of cutoff *L*-shells are given.

Data Availability Statement

Data Availability Statement Global Positioning System and Geostationary Operational Environmental Satellites (GOES) energetic particle data is available through the online archives of the National Centers for Environmental Information of the National Oceanic and Atmospheric Administration, Boulder, USA. GPS: <https://www.ngdc.noaa.gov/stp/space-weather/satellite-data/satellite-systems/gps/> (version v1.08) and GOES: <https://www.ngdc.noaa.gov/stp/satellite/goes/> (used for GOES integral >10 MeV proton fluxes). In addition, the Solar Energetic Particle Environment Modelling Reference Data Set Version 2.1 (interpolated proton fluxes with background fluxes subtracted and spikes and other corrupted data removed or corrected) can be found here: http://sepem.eu/help/SEPEM_RDS_v2-01.zip. The *Dst* (<https://doi.org/10.17593/14515-74000>) and *Kp* (<https://doi.org/10.5880/Kp.0001>) indices are available at WDC for Geomagnetism, Kyoto, Japan: <http://wdc.kugi.kyoto-u.ac.jp/wdc/Sec3.html>. The solar wind data was obtained from https://omniweb.gsfc.nasa.gov/form/omni_min.html.

Acknowledgments

We thank Steven K. Morley and Amanda Stricklan for discussion the Combined X-ray Dosimeters (CXD) data with us. The funding support for C.M. van Hazendonk and E. Heino is provided by the Norwegian Research Council (NRC) under contract number 287427. The work of C.M. van Hazendonk has further been supported by the NRC under CoE contract 223252/F50. In addition, the work of N. Partamies is supported by NRC under CoE contract 223252. We acknowledge the work of the CXD team at Los Alamos National Laboratory on the energetic particle data from Global Positioning System, ESA's Solar Energetic Particle Environment Modeling team as well as National Oceanic and Atmospheric Administration, Boulder, USA for the work on Geostationary Operational Environmental Satellites energetic particle data, WDC for Geomagnetism, Kyoto, Japan, for providing the *Dst* index, GFZ German Research Centre for Geosciences, Potsdam, Germany, for providing the *Kp* index and SPDF Goddard Space Flight Center, Greenbelt, USA for the work on the solar wind parameters.

References

- Birch, M. J., Hargreaves, J. K., Senior, A., & Bromage, B. J. I. (2005). Variations in cutoff latitude during selected solar energetic proton events. *Journal of Geophysical Research*, *110*(A7). <https://doi.org/10.1029/2004JA010833>
- Boschini, M. J., Della Torre, S., Gervasi, M., Grandi, D., La Vacca, G., Rancoita, P. G., et al. (2021). A quantitative study on the effects of external geomagnetic fields by using the geomagsphere back-tracing code. *Advances in Space Research*, *68*(7), 2904–2918. <https://doi.org/10.1016/j.asr.2021.05.022>
- Carver, M., Morley, S. K., & Stricklan, A. (2020). GPS constellation energetic particle measurements. *IEEE Aerospace conference* (pp. 1–10). <https://doi.org/10.1109/AERO47225.2020.9172652>
- Carver, M. R., Sullivan, J. P., Morley, S. K., & Rodriguez, J. V. (2018). Cross calibration of the GPS constellation CXD proton data with GOES EPS. *Space Weather*, *16*(3), 273–288. <https://doi.org/10.1002/2017SW001750>
- Cayton, T. (2004). *Monte Carlo simulation of the particle channels of the combined X-ray and dosimeter (CXD)*. (Tech. Rep. No. LA-UR-04-7092). Los Alamos: Los Alamos National Laboratory. Retrieved from <http://permalink.lanl.gov/object/tr?what=info:lanl-repo/lareport/LA-UR-04-7092>
- Chen, Y., Morley, S. K., & Carver, M. R. (2020). Global prompt proton sensor network: Monitoring solar energetic protons based on GPS satellite constellation. *Journal of Geophysical Research: Space Physics*, *125*(3), e2019JA027679. <https://doi.org/10.1029/2019JA027679>
- Distel, J. C., Blair, S. G., Cayton, T. E., Dingler, R. D., Guyker, F., Ingraham, J. C., & Wehner, T. J. (1999). *The Combined X-ray Dosimeter CXD on GPS block IIR satellites*. Tech. Rep. No. LA-UR-99-2280. Los Alamos National Laboratory. Retrieved from <https://permalink.lanl.gov/object/tr?what=info:lanl-repo/lareport/LA-UR-99-2280>
- Dmitriev, A. V., Jayachandran, P. T., & Tsai, L.-C. (2010). Elliptical model of cutoff boundaries for the solar energetic particles measured by POES satellites in December 2006. *Journal of Geophysical Research*, *115*(A12). <https://doi.org/10.1029/2010JA015380>
- Durante, M., & Cucinotta, F. A. (2011). Physical basis of radiation protection in space travel. *Reviews of Modern Physics*, *83*, 1245–1281. <https://doi.org/10.1103/RevModPhys.83.1245>
- Ganushkina, N. Y., Liemohn, M. W., & Dubyagin, S. (2018). Current systems in the Earth's magnetosphere. *Reviews of Geophysics*, *56*(2), 309–332. <https://doi.org/10.1002/2017RG000590>
- Heino, E. (2019). *Spatial extent of solar proton impact in the Earth's atmosphere: Observations and modeling (unpublished doctoral dissertation)*. UiT The Arctic University of Norway. Available at <https://hdl.handle.net/10037/16914>
- Jiggins, P., Clavie, C., Evans, H., O'Brien, T. P., Witasse, O., Mishev, A. L., et al. (2019). In situ data and effect correlation during September 2017 solar particle event. *Space Weather*, *17*(1), 99–117. <https://doi.org/10.1029/2018SW001936>
- Kress, B. T., Mertens, C. J., & Wiltberger, M. (2010). Solar energetic particle cutoff variations during the 29–31 October 2003 geomagnetic storm. *Space Weather*, *8*(5). <https://doi.org/10.1029/2009SW000488>
- Leske, R. A., Mewaldt, R. A., Stone, E. C., & von Roseninge, T. T. (2001). Observations of geomagnetic cutoff variations during solar energetic particle events and implications for the radiation environment at the space station. *Journal of Geophysical Research*, *106*(A12), 30011–30022. <https://doi.org/10.1029/2000JA000212>
- Matthes, K., Funke, B., Andersson, M. E., Barnard, L., Beer, J., Charbonneau, P., et al. (2017). Solar forcing for CMIP6 (v3.2). *Geoscientific Model Development*, *10*(6), 2247–2302. <https://doi.org/10.5194/gmd-10-2247-2017>
- Matzka, J., Bronkalla, O., Tornow, K., Elger, K., & Stolle, C. (2021). Geomagnetic Kp index. V. 1.0. GFZ Data Services. <https://doi.org/10.5880/Kp.0001>
- Morley, S. K., Sullivan, J. P., Carver, M. R., Kippen, R. M., Friedel, R. H. W., Reeves, G. D., & Henderson, M. G. (2017). Energetic particle data from the Global Positioning System constellation. *Space Weather*, *15*(2), 283–289. <https://doi.org/10.1002/2017SW001604>
- Morley, S. K., Sullivan, J. P., Henderson, M. G., Blake, J. B., & Baker, D. N. (2016). The Global Positioning System constellation as a space weather monitor: Comparison of electron measurements with Van Allen Probes data. *Space Weather*, *14*(2), 76–92. <https://doi.org/10.1002/2015SW001339>
- Neal, J. J., Rodger, C. J., & Green, J. C. (2013). Empirical determination of solar proton access to the atmosphere: Impact on polar flight paths. *Space Weather*, *11*(7), 420–433. <https://doi.org/10.1002/swe.20066>
- Nesse Tyssøy, H., & Stadsnes, J. (2015). Cutoff latitude variation during solar proton events: Causes and consequences. *Journal of Geophysical Research: Space Physics*, *120*(1), 553–563. <https://doi.org/10.1002/2014JA020508>
- Nesse Tyssøy, H., Stadsnes, J., Søråas, F., & Sørbo, M. (2013). Variations in cutoff latitude during the January 2012 solar proton event and implication for the distribution of particle energy deposition. *Geophysical Research Letters*, *40*(16), 4149–4153. <https://doi.org/10.1002/grl.50815>
- Nose, M., Sugiura, M., Kamei, T., Iyemori, T., & Koyama, Y. (2015). *Dst Index (Version 1.0)* [Data set]. WDC for Geomagnetism. <https://doi.org/10.17593/14515-74000>
- O'Brien, T. P., Mazur, J. E., & Looper, M. D. (2018). Solar energetic proton access to the magnetosphere during the 10–14 September 2017 particle event. *Space Weather*, *16*(12), 2022–2037. <https://doi.org/10.1029/2018SW001960>
- Onsager, T., Grubb, R., Kunches, J., Matheson, L., Speich, D., Zwickl, R. W., & Sauer, H. (1996). Operational uses of the GOES energetic particle detectors. In E. R. Washwell (Ed.), (Vol. 2812, pp. 281–290). *GOES-8 and Beyond*. SPIE. <https://doi.org/10.1117/12.254075>

- Reames, D. V. (1999). Particle acceleration at the Sun and in the heliosphere. *Space Science Reviews*, 90(3), 413–491. <https://doi.org/10.1023/A:1005105831781>
- Rodriguez, J. V., Onsager, T. G., & Mazur, J. E. (2010). The east-west effect in solar proton flux measurements in geostationary orbit: A new GOES capability. *Geophysical Research Letters*, 37(7). <https://doi.org/10.1029/2010GL042531>
- Smart, D., & Shea, M. (2003). The space-developed dynamic vertical cutoff rigidity model and its applicability to aircraft radiation dose. *Advances in Space Research*, 32(1), 103–108. [https://doi.org/10.1016/S0273-1177\(03\)90376-0](https://doi.org/10.1016/S0273-1177(03)90376-0)
- Smart, D., & Shea, M. A. (2001). A comparison of the Tsyganenko model predicted and measured geomagnetic cutoff latitudes. *Advances in Space Research*, 28(12), 1733–1738. [https://doi.org/10.1016/S0273-1177\(01\)00539-7](https://doi.org/10.1016/S0273-1177(01)00539-7)
- Smart, D., & Shea, M. A. (2005). A review of geomagnetic cutoff rigidities for Earth-orbiting spacecraft. *Advances in Space Research*, 36, 2012–2020. <https://doi.org/10.1016/j.asr.2004.09.015>
- Smart, D., Shea, M. A., & Flückiger, E. (2000). Magnetospheric models and trajectory computations. *Space Science Reviews*, 93, 305–333. <https://doi.org/10.1023/A:1026556831199>
- Smart, D., Shea, M. A., & Gall, R. (1969). The daily variation of trajectory-derived high-latitude cutoff rigidities in a model magnetosphere. *Journal of Geophysical Research*, 74(19), 4731–4738. <https://doi.org/10.1029/JA074i019p04731>
- Störmer, C. (1955). *The polar aurora*. Clarendon Press.
- Tuszewski, M., Cayton, T. E., Ingraham, J. C., & Kippen, R. M. (2004). Bremsstrahlung effects in energetic particle detectors. *Space Weather*, 2(10). <https://doi.org/10.1029/2003SW000057>
- Verronen, P. T., Kero, A., Partamies, N., Szelag, M. E., Oyama, S.-I., Miyoshi, Y., & Turunen, E. (2021). Simulated seasonal impact on middle atmospheric ozone from high-energy electron precipitation related to pulsating aurorae. *Annales Geophysicae*, 39(5), 883–897. <https://doi.org/10.5194/angeo-39-883-2021>